Pharmaceutical Research, Vol. 23, No. 4, April 2006 (© 2006)
DOI: 10.1007/s11095-006-9748-0

Research Paper

Oligonucleotide–Polyethylenimine Complexes Targeting Retinal Cells: Structural Analysis and Application to Anti-TGFβ-2 Therapy

Ana L. Gomes dos Santos,[1,2,3] Amélie Bochot,[2] Nicolas Tsapis,[2] Franck Artzner,[4] Riad Antoine Bejjani,[1] Brigitte Thillaye-Goldenberg,[1] Yvonne de Kozak,[1] Elias Fattal,[2] and Francine Behar-Cohen[1,5]

Received October 21, 2005; accepted December 14, 2005

Purpose. The aim of this study was to characterize oligonucleotide–polyethylenimine (ODN/PEI) complex preparation for potential transfection of retinal cells *in vitro* and *in vivo*.
Methods. The effect of medium preparation [HEPES-buffered saline (HBS), water] on particle size and morphology was evaluated. Cultured Lewis rat retinal Müller glial (RMG) cells were transfected using fluorescein isothiocyanate (FITC)–ODN/PEI complexes specifically directed at transforming growth factor beta (TGFβ)-2. Efficacy of transfection was evaluated using confocal microscopy, and regulation of gene expression was assayed using quantitative real-time RT-PCR and ELISA assay. One, 24, and 72 h after injection of FITC–ODN/PEI complexes into the vitreous of rat eyes, their distribution was analyzed on eye sections.
Results. Complexes prepared in HBS were smaller than complexes prepared in pure water and presented a core–shell structure. These particles showed a high cellular internalization efficacy, along with a significant and specific down-regulation of TGFβ-2 expression and production in RMG cells, correlating with specific inhibition of cell growth at 72 h. *In vivo*, complexes efficiently transfect retinal cells and follow a transretinal migration at 24 h. After 72 h, ODN seems to preferentially target RMG cells without inducing any detectable toxicity.
Conclusions. Specific down-regulation of TGFβ-2 expression using ODN/PEI complexes may have potential interest for the treatment of retinal diseases associated with glial proliferation.

KEY WORDS: antisense; oligonucleotides; polyethylenimine; retinal Müller glial cells; TGFβ-2.

INTRODUCTION

Effective implementation of gene regulation using oligonucleotide (ODN) technology in biology is hampered by low gene transfection efficacy. Because ODNs are charged molecules of high molecular weight, their transportation across cell membranes is poor (1,2). To improve gene delivery, different systems have been developed including cationic liposomes (3,4), polycationic dendrimers (5), cationic peptides (6), cationic polymers such as polyethylenimine (PEI) (7–9), microspheres, and nanoparticles (10,11).

The eye is an attractive target for antisense therapeutic strategies. The volume of tissue to be treated is relatively small and easily accessible. The presence of ocular–blood barriers limits the diffusion of active drugs from the eye to the circulation, allowing a potentially effective local therapy. On the other hand, systemic delivery has a low intraocular penetration. Interestingly, the first FDA-approved clinical application of antisense strategy has been the treatment of cytomegalovirus (CMV) retinitis using intravitreous injection of phosphorothioate specific antisense oligonucleotides (7). To limit nucleic acid degradation in the vitreous, their potential toxicity, and improve their intraretinal penetration, different options have been evaluated, particularly encapsulation within liposomes (8,9) or in polymeric particles (10).

Transforming growth factor beta (TGFβ)-2 plays a pivotal role in the regulation of ocular disease manifestation, markedly influencing those associated with glial proliferation (11). Among these retinal diseases, proliferative vitreoretinopathy (PVR), characterized by the formation of retractile fibrosis on both surfaces of the retina and in the vitreous cavity, is a major cause of retinal detachment surgery failure (12). Retinal pigment epithelial cells, fibroblasts, macrophages, and retinal Müller glial (RMG) cells have been involved in this pathological process (13–15). In the eye, TGFβ isoforms are predominantly found in the vitreous of patients with PVR (16–18). Also, neutralization of TGFβ-2 activity using adenovirus-mediated transfection of a soluble TGFβ-2 receptor type II reduced the severity of proliferative vitreoretinopathy (19).

[1] INSERM U 598, 15 rue de l'Ecole de Médecine, 75270 Paris, Cedex 06, France.
[2] Laboratoire de Physico-Chimie, Pharmacotechnie, Biopharmacie, UMR CNRS 8612, Châtenay-Malabry, Cedex, France.
[3] Departamento de Ciencias Farmaceuticas, Universidade Federal de Santa Catarina (UFSC), Florianopolis, SC, Brazil.
[4] Laboratoire de Physique de la Matière Condensée, Unité Mixte de Recherche 6626, Université de Rennes 1, Rennes, France.
[5] To whom correspondence should be addressed. (e-mail: behar@idf.inserm.fr)

In this study, we investigated the morphology and structure of oligonucleotides (ODN)/polyethylenimine (PEI) complexes, prepared in different medium solutions. The structure of the complexes was related to their biocompatibility and their ability to specifically down regulate TGFβ-2 expression in rat RMG cells *in vitro* and their behavior *in vivo*.

MATERIALS AND METHODS

All culture reagents were obtained from Invitrogen (Cergy Pontoise, France). Polyethylenimine (PEI, Mw 25,000 Da, Mn 10,000, branched) was purchased from Aldrich (Ingelheim, Germany). The TGFβ-2 antisense oligodeoxynucleotide (As-ODN), full phosphorothioate, 5′ end covalently conjugated or not with fluorescein isothiocyanate (FITC) was purchased from PROLIGO (Paris, France). We used the anti TGFβ-2 ISIS 123285 sequence (20) 5′-CCG TGA CCA GAT GCA GGA T-3′ (19 mer) and the control scrambled ODN (Sc-ODN) sequence 5′-TAT CGA GGG ATA GCA CCC G-3′. All other chemicals, unless stated otherwise, were obtained from Sigma (St-Quentin Fallavier, France).

Preparation of Complexes

ODN/PEI complexes were formed at three different molar ratios (5, 10, and 15) of PEI nitrogen to ODN phosphate (N/P ratio). ODN aqueous solution was prepared at a concentration of 20 mg/ml (w/v), as well as a stock aqueous solution of PEI (60 mg/ml, pH adjusted to 7). PEI and ODN solutions were freshly diluted in HEPES-buffered saline (HBS) (10 mM HEPES, 150 mM NaCl, pH 7.4) or pure water (Milli-Q) to obtain the desired concentrations. ODN/PEI complexes were prepared by vortexing equal volumes (200 μL) of PEI with ODN solutions for 2 min. The final ODN concentration was in the range of 0.25–1.0 mg/ml, which corresponds to 40–160 μM.

Complex Characterization

Amount of Complexed Oligonucleotide

The amount of ODN complexed by PEI was quantified by UV spectrophotometry at a wavelength of 260 nm (Perkin-Elmer UV/V is spectrophotometer, Lambda 11, Foster, CA, USA) (21). Briefly, complexes were prepared as described previously, incubated for 15 min at room temperature, and centrifuged at 2900 × *g* for 30 min. For each sample, the pellet was dissolved into 0.5 N NaOH under magnetic stirring at 37°C. The ODN present in the pellet and in the supernatant was then quantified.

Size and Zeta Potential Measurements

Complex size and polydispersity were determined in triplicate by quasi-elastic light scattering using a Nanosizer Coulter N4 (Beckman Coulter, Roissy, France) at 20°C and at an angle of 90°. Samples were diluted in pure water or in HBS according to the preparation medium to satisfy the detection range of the device.

The electrophoretic mobility of complexes prepared either in water or in HBS was measured at 25°C with a Malvern Zetasizer 4 (Malvern Instruments, Malvern, UK) following 1/50 dilution in HEPES buffer (10 mM, pH 7.4).

Stability of the Size Particles in Transfection Medium

The influence of transfection medium complexes on size was studied by incubating the particles in transfection culture medium. Particles prepared in water or HBS (1 mg/mL; N/P = 10) were diluted in 1/10 reduced serum medium (Opti-MEM I) and incubated at 37°C. Samples were taken after 5, 30, 60, 120, 180, and 220 min and particle sizes were determined by quasi-elastic light scattering.

Morphology of Complexes

Transmission Electron Microscopy

Ten microliters of complexes diluted to 1/10 prepared in pure water or in HBS was deposited on copper grids covered with a formvar film (400 mesh) for 2 min. Excess solution was blotted off using filter paper, and grids were stained using 5 μL of aqueous uranyl acetate 1% (w/v) for 2 min. Excess staining solution was blotted off using filter paper, and grids were air-dried. Preparations were observed under a JEM 1200 EX (Jeol-France, Roissy, France) transmission electron microscope (TEM) operating at 80 kV.

Scanning Electron Microscopy

The complexes morphology was observed using a LEO 1530 scanning electron microscope (SEM) equipped with a Gemini column (PGT, USA). Ten microliters of each sample was deposited onto a piece of double-sided carbon tape coating an aluminum stub. Samples were sputter-coated with gold (thickness 2 nm).

Freeze-Fracture Electron Microscopy

Electron microscopy observations were preceded by freeze-fracture (FFEM) of samples containing 30% glycerol (cryoprotector). Samples were placed on a copper holder and then snap-frozen into liquid propane. Frozen samples were fractured under vacuum (10−7 Torr) with a single-edge scalpel maintained at 77 K. Freeze fracture and replication were successively performed using a Balzers BAF 400T apparatus (BAL-TEC, Balzers, Liechtenstein). Replication of the surface exposed to freeze fracture was achieved in two steps: 2 nm of platinum was evaporated from an oblique angle (45°) to provide contrast enhancement of the surface topology; a thicker continuous layer (20 nm) of an electron transparent material (carbon) was then deposited under an angle of 90°. The carbon layer allowed strengthening of the replica. Layer thickness was controlled by a quartz crystal gauge. Replicas were then washed using water to eliminate the underlying sample. Replicas were examined using a LEO 912 electron microscope equipped with an omega filter working at 120 kV.

Light Microscopy

Preparations were placed between glass slides and observed with an Olympus IX70 inverted microscope equipped with cross-polarizer and a dark field condenser (22). A 4410 COHU camera was used to detect the low light intensity.

IN VITRO STUDIES

Preparation of Rat Retinal Müller Glial Cells

All usage of animals adhered to the ARVO statement for the Use of Animals in Ophthalmic and Vision Research. RMG cells were isolated from Lewis rat retinas on postnatal day 8 as previously described (23). Briefly, eyeballs from decerebrated young rats were incubated in Dulbecco's modified Eagle's medium (DMEM) containing 0.2% trypsin (Difco, Detroit, MI, USA) and 100 U/mL collagenase type CS-1 (Worthington, Freehold, NJ, USA). The neural retinas were separated from the lens and vitreous, cut into small fragments, and plated in 100-mm petri dishes in DMEM containing 10% fetal bovine serum (FBS) and antibiotic (100 U/mL penicillin). After 3 to 4 days, fragments were removed by extensive rinsing with phosphate-buffered saline (PBS), and the remaining flat cell population was fed with DMEM. When these RMG cell cultures reached near confluency, they were harvested and frozen.

INTERNALIZATION OF COMPLEXES AND TRANSFECTION OF ODN INTO RMG CELLS

After 24 h of culture in DMEM/10% FBS at 37°C (5% CO_2), RMG cells (25×10^3 cells plated on four-well culture slides) were washed with PBS and incubated with 250 μL of 200 nM (ODN) complexes prepared in water or in HBS (1 mg/mL), or with naked ODN (FITC-labeled ODN) in Opti-MEM for 6 h. After incubation, cells were washed with PBS and fixed with 4% paraformaldehyde. The number of cells having internalized particles was counted using a fluorescent microscope (Aristoplan, Leica, Heidelburg, Germany). Representative pictures of the cells were taken using a confocal microscope (as described below).

To evaluate the intracellular stability of complexes prepared in HBS, 6 h after incubation in Opti-MEM, cells were washed in PBS and further cultured in DMEM 10% for 24 or 72 h. Cells were then washed with PBS, fixed, mounted, and observed using a confocal microscope equipped with a Plan-Apochromat 63X/1.4 NA oil-immersion objective lens (Zeiss, Jena, Germany). The pinhole was set at 1 Airy unity. Fluorescence images were acquired with argon (wavelength 488 nm). Differential interference contrast (DIC) was used to visualize the cells.

Cell Viability and Proliferation

RMG cell viability was assessed using the 3-(4, 5-dimethylthiazol-2-yl)-2, 5-diphenyltetrazolium bromide (MTT) test after 6 h of incubation with complexes or naked ODN ranging from 50 to 400 nM and PEI from 4.75 to 38 μM. The amount of free PEI used to evaluate cell viability was similar to the amount used to form the complexes at different concentrations.

Twenty-four hours before transfection, 20×10^3 RMG cells/well (24-well plate) were grown in DMEM 10%/FBS. Cells were washed twice with PBS and medium replaced by 250 μL of Opti-MEM containing increasing concentrations of complexes (HBS), ODN, or PEI. After 6 h incubation, cells were washed twice with PBS incubated in 100 μL of MTT/well (1 mg/mL in PBS containing 1 g/L glucose) for 1 h at 37°C. The resulting insoluble formazan crystals were dissolved in 100 μL of propanolol. The optical density was determined in a plate reader set at 450 nm with wavelength correction set at 540 nm (Bio-Rad Model 450, Marnes-la-Coquette, France).

To evaluate potential growth inhibition of cells that have been exposed to complexes (100 and 200 nM, prepared with antisense and scrambled ODNs) for 6 h, the number of living cells was also quantified in a separate experiment at 72 h. For this purpose, after 6 h of treatment, cells were washed and incubated in new medium for 66 additional hours as previously described and then processed for MTT assay.

Tests were conducted in three to six replicates for each concentration. Results are expressed as relative cell viability using a standard curve for each experiment.

TGFβ-2 Expression and Production by RMG Cells

After 24 h of culture in DMEM/10% FBS at 37°C (5% CO2), RMG seeded in a six-well plate at 12×10^4 cells/well were washed twice with Opti-MEM. Solutions of freshly prepared complexes (HBS), naked ODN, or PEI were diluted in Opti-MEM to 200 nM, added to the cultures and incubated at 37°C for 6 h. Opti-MEM was then replaced by growth medium and the cultures further incubated for 72 h. Following this last incubation, culture supernatants were collected to dose TGFβ-2 and cells were harvested and processed for real time RT-PCR.

Real Time RT-PCR

Total RNA was isolated from RMG cells using a RNA easy Mini kit (Qiagen, Les Ulis, France). The concentration and the purity of all RNA samples were determined by measuring their absorbance by spectrometry at 260 and 280 nm (DU®-640 3 UV/Vis spectrophotometer, Beckman Coulter, Fullerton, CA, USA).

To assess integrity and concentration of the total RNA, 1 μL was directly analyzed on an RNA 6000 Nano LabChip (Agilent, Wilmington, DE, USA) following the manufacturer's instructions.

First-strand cDNA was generated by reverse transcription of 250–1000 ng of total RNA using oligo(deoxythimidine) 12–18 primer and Superscript™ II RNase H reverse transcriptase (Invitrogen, Cergy Pontoise, France) according to the manufacturer's instructions, in a total reaction volume of 20 μL. Negative controls of the cDNA templates were prepared either without the RNA or without the reverse transcriptase and produced no amplification in the PCR assay.

Quantification of the TGFβ-2 transcripts was performed by real-time PCR on a LightCycler® thermal cycler (Roche

Table I. Primer Sets for Quantitative Real-Time PCR Used for mRNA Quantification

Gene	GenBank accession no.	Nucleotide	Amplicon size (bp)	Forward primer (5′–3)′	Reverse primer (5′–3)′
GAPDH	NM_017008	895–1062	168	gttaccagggctgccttctc	gggtttcccgttgatgacc
TGFβ-2	NM_031131	746–940	195	ccgcccactttctacagaccc	gcgctgggttggagatgttag

Diagnostics, Meylan, France). A cDNA amount synthesized from total RNA was amplified in a PCR mixture containing the FastStart DNA Master SYBR® Green I reagent (Roche Diagnostics), 5 mM $MgCl_2$ and 0.5 μM of each primer (Table I). After an 8-min hot start at 95°C, amplification was allowed to proceed for 45 cycles each consisting of denaturation at 95°C for 5 s, annealing at 55°C for 5 s, and extension at 72°C for 9 s. To check the amplification specificity, the PCR product was subjected to a melting curve analysis and an agarose gel electrophoresis. These fragments were purified using the High Pure PCR Product Purification Kit (Roche Diagnostics), quantified spectrophotometrically, and sequenced (MWG Biotech, Courtaboeuf, France). The C_t values were calculated using the second-derivative maximum algorithm provided by the Light Cycler software. Five serial dilutions of cDNA from the positive control RMG cells were analyzed to allow the construction of the calibration curve C_t *vs.* log (cDNA input in PCR) from which quantities within samples were calculated. Quantities of target sequences were expressed in nanograms for 100 ng of reverse-transcribed RNA. All PCR efficiencies (E), calculated from the slopes of the standard curves according to the equation $E = [10(-1/\text{slope})] - 1$, were higher than 90%. Quantitative PCR data for each gene were graphed as fold activation values, normalized to the glyceraldehyde-3-phosphate dehydrogenase (GAPDH) mRNA content of each cDNA. Mean values ± SD from two or three separate experiments are presented.

TGFβ-2 Levels using ELISA

The levels of TGFβ-2 were evaluated by ELISA using Quantikine® enzyme immunological ELISA kits (R & D Systems, Minneapolis, MN, USA) according to the manufacturer's instruction. Optical density was determined in a plate reader set at 450 nm with wavelength correction set at 570 nm (Bio-Rad Model Benchmark Plus). Linearity of TGFβ-2 calibration curve was ensured between 15.6 and 1000 pg of TGFβ-2/mL (r^2 = 0.9995). Data are presented as means ± standard errors derived from three to four experiments.

IN VIVO STUDIES

Fate of ODN/PEI Complexes *in Vivo*

To evaluate the biodistribution of ODN/PEI complexes *in vivo*, 10 μL of complexes prepared in HBS of FITC–ODN (50 μM)/PEI were injected into the vitreous of 12 Lewis female rats (6 weeks old) as previously described (24). Control rats received 10 μL/eye of naked FITC ODN (50 μM) (n = 6). At 1 and 24 h and 3 days after injection (n = 2 per time point), rats were examined using a slit-lamp (Haag Streit, Wedel, Germany) to evaluate clinical tolerance and were then killed by use of a lethal dose of pentobarbital. Enucleated eyes were fixed for 2 h in 4% paraformaldehyde and included in OCT for cryosection. Ten-micrometer cross sections at the optic nerve head level were collected on gelatin-coated slides, rinsed in PBS twice, stained with 4′, 6-diamino-2-phenylindole (DAPI) (1:3000) and mounted using PBS/glycerol (1:1). Sections were examined using a fluorescence microscope Aristoplan (Leica, Rueil-Malmaison, France) and photographed with a Spot RT digital camera (Optilas, Every, France). Other sections were stained with hematoxylin–eosin for tolerance analysis.

Immunohistochemistry

To identify glial cells on eye sections of rat eyes, slides were incubated for 1 h at 20–22°C with monoclonal anti-GFAP (Serotec, Varilhes, France) diluted 1/100 in PBS. After washing, sections were incubated in a solution of 1/100 of secondary goat anti-rabbit antibody conjugated to Alexa (Molecular Probes, Interchim, Asnières, France) for 1 h. The slides were then washed, stained for 5 min with DAPI solution diluted 1/3000 (Sigma-Aldrich, St-Quentin Fallavier, France), washed again in PBS and mounted in glycerol/PBS (1:1). Stained sections were viewed with a fluorescence microscope Aristoplan (Leica) and photographed with a Spot RT digital camera (Optilas). Experiments using nonimmune serum or omitting the first antibody served as controls. Each staining was performed on a minimum of three independent samples.

Statistical Analysis

Results were expressed as means ± SD and the statistical analysis was performed using the nonparametric Mann–Whitney U test. A value of $p < 0.05$ was considered as significant.

RESULTS

Complex Characterization

Amount of Complexed ODNs, Size, and Zeta Potential

To determine the percentage of PS-ODN associated within complexes (1 mg/mL) the amount of PS-ODN in the pellet and in the supernatant was assessed after centrifugation. For all samples, 98–100% of PS-ODN was found in the pellet. PS-ODN was therefore fully complexed by PEI in the N/P ratio range chosen.

Particle size, polydispersity index (PI), and zeta potential of ODN/PEI complexes were measured as a function of three parameters: N/P ratio, ODN concentration, and preparation medium.

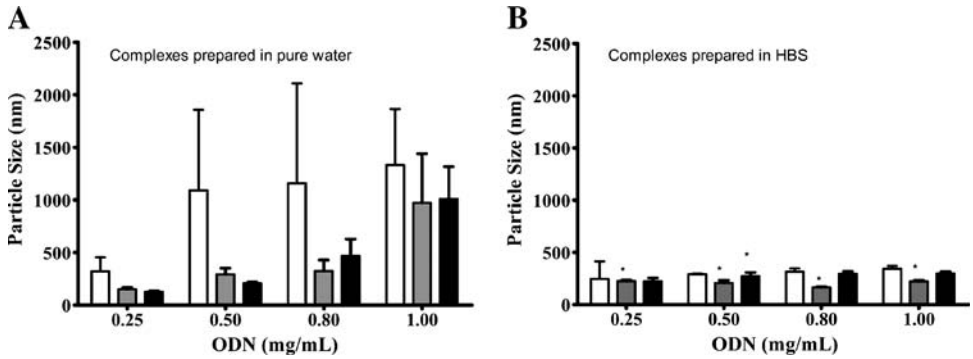

Fig. 1. Size of ODN/PEI complexes. Samples were prepared at different N/P ratios (□) 5, (■) 10 and (■) 15; different ODN concentrations (0.25, 0.50, 0.80 and 1.0 mg/mL, which correspond to 40, 80, 128 and 160 μM) and in different preparation media: Milli-Q water (1A) or HBS (1B). All samples prepared in pure water exhibit polydispersity indices greater than 0.2, whereas samples in HBS have polydispersity indices ≤0.2 noted with *.

Figure 1 illustrates the effect of preparation medium on the size and polydispersity of complexes. For samples prepared in water, size increases as a function of the ODN concentration and reaches the micrometer range at a concentration of 1 mg/mL (Fig. 1A). A very broad particle size distribution (PI > 0.2) was noted for all water medium preparations. In contrast, samples prepared in HBS present substantial differences. Most importantly, particle size remains constant in the range of 150 to 350 nm even at high ODN concentration (Fig. 1B). In addition, polydispersity indices for N/P ratio 10 are always smaller than 0.2, clearly indicating a monodisperse size distribution. Size and PI of these complexes were stable over 6 h. The zeta potential of complexes prepared in water and HBS exhibit a constant positive charge of +16 to +24 mV, respectively.

After 4 h of incubation in Opti MEM, the size of complexes (1 mg/mL) prepared in pure water was around 1 μm, whereas the size of complexes prepared in HBS remained at about 300 nm.

Morphology and Structure of the Complexes

Using different microscopic techniques (SEM, TEM, FFEM dark-field and polarized optical microscopy), the morphological and structural characteristics of the complexes prepared in water or HBS were analyzed (Fig. 2). The size of

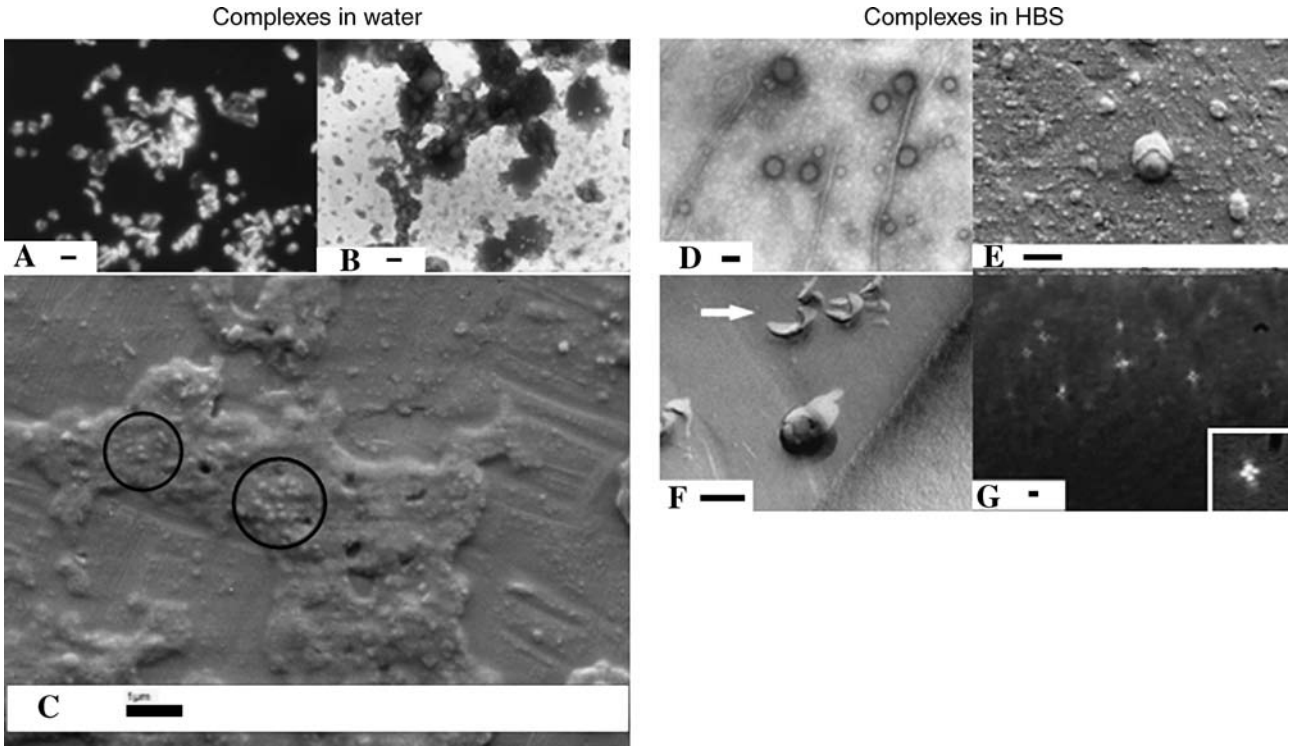

Fig. 2. Morphology of ODN/PEI complexes (N/P ratio = 10 and ODN concentration = 1 mg/mL). (A–C) complexes prepared in water: Dark field optical micrograph (A), TEM micrograph (B) and SEM micrograph (C). Scale bars: A = 5 μm, B = 100 nm and C = 1 μm. (D–G) Complexes prepared in HBS: TEM micrograph (D), SEM micrograph (E), FFEM micrograph (F), polarized optical micrograph (G). Scale bars: D and F = 100 nm; B = 500 nm and G = 2 μm (insert is magnified twice as compared to the picture).

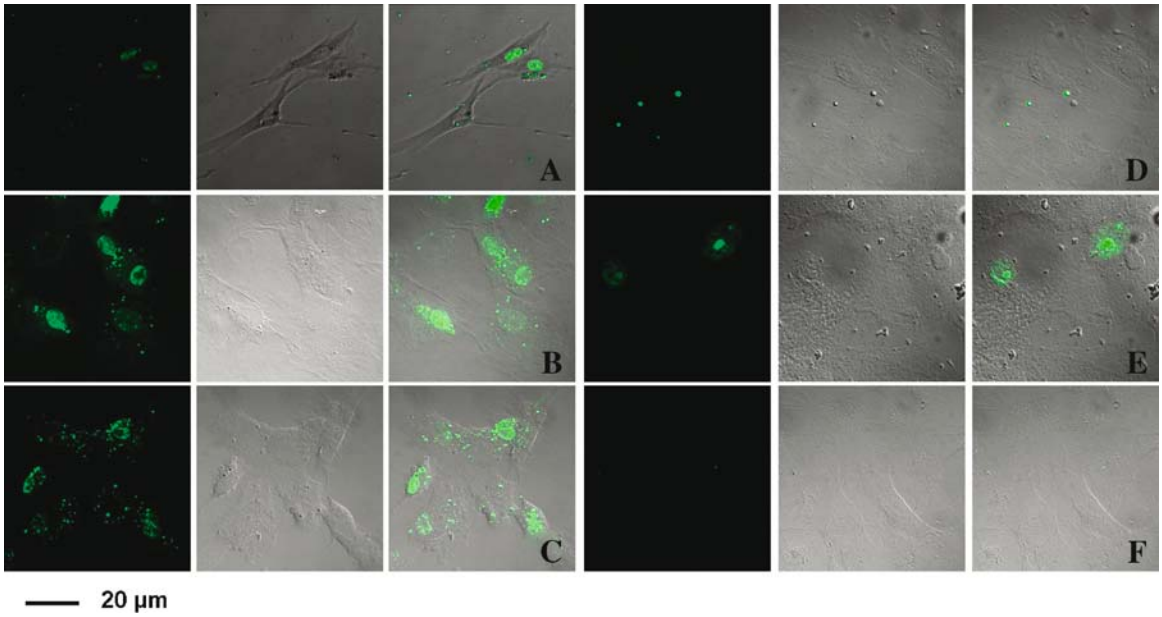

Fig. 3. Confocal photomicrographs of the uptake of complexes and naked ODN (FITC-labelled ODN) on RMG cells, for 6, 24 and 72 hours after incubation (200 nM). For each sample three micrographs were taken: (left-hand side) green-Fluorescent; (middle side) Differential Interference Contrast; (right-hand side) overlap of the two previous images. (A–C): Photomicrographs from cells incubated with complexes prepared in HBS 6 hours (A), 24 hours (B) and 72 hours (C) after incubation. (D): Photomicrographs from cells incubated with complexes prepared in water 6 hours after incubation. (E–F): Photomicrographs from cells incubated with naked ODN (E) 6 hours and (F) 24 hours after incubation. Bar = 20 µm.

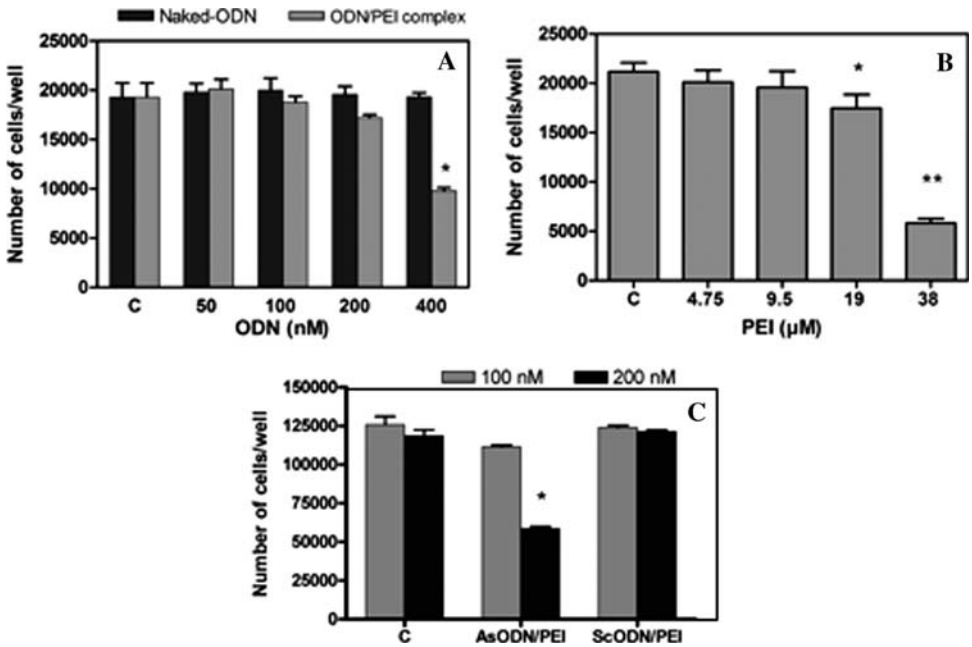

Fig. 4. RMG Cell viability after 6 hours of incubation with complexes, naked ODN and PEI (MTT assay). Complexes were diluted in Opti-MEM to obtain the desired concentrations. PEI and naked ODN concentrations were relative to those present in complex formation. (A) Cells were incubated with naked ODN (□) or with complexes (■), ranging from 50 to 400 nM (*P = 0.01). (B) PEI concentration (◇), ranging from 4.75 µM to 38 µM (*P = 0.03; **P = 0.0001). Results are expressed as percentages of control (untreated cells). Data are the mean ± SD. PEI and naked ODN concentrations were relative to those present in complexes. (C) Number of RMG cells at 72 hours after treatment with complexes (ODN/PEI): antisenseTGFβ-2 oligonucleotides (AsODN/PEI), scrambled control sequence (ScODN/PEI), ODN concentrations were 100 and 200 nM which correspond to 9.5 and 19 µM of PEI, respectively. Results are expressed as percentages of control (untreated cells). Data are the mean ± SD out of three samples. *Statistically significant difference *versus* control (*P = 0.004). There is no difference between control cells and cells treated with scramble sequence complexes (P > 0.5).

the particle aggregates as assessed by optical microscopy is a few microns (Fig. 2A). This observation was confirmed by TEM (Fig. 2B) and SEM micrographs (Fig. 2C). Close analysis of SEM images shows that these aggregates are made up of several small particles (20–50 nm) forming a network structure (Fig. 2C).

In contrast, for complexes prepared in HBS, the TEM micrograph shows isolated spherical particles having a diameter of 100 to 200 nm (Fig. 2D). Surface details seen through SEM (Fig. 2E) show the presence of a shell wrapped around a spherical particle (Fig. 2E). In line with this observation, the FFEM micrograph (Fig. 2F) reveals dense spherical particles (diameter about 100 nm) as well as the remaining of a shell-like structure (arrow). Finally, by cross-polarizing microscopy, only the largest particles (about 2 μm) can be observed (Fig. 2G): the Malta cross images, which are commonly observed with multilamellar vesicles, proves the nanoparticle spherical symmetry.

IN VITRO STUDIES

ODN and Complexes Uptake

Six hours after incubation of the cell cultures with HBS-generated complexes, FITC–ODN/PEI nanoparticles are identified in about 70% of the RMG cells as fluorescent bodies within the cytoplasm. Intense fluorescence is also located in the cell nuclei (Fig. 3A). The fluorescent nanoparticles are still observed in the cytoplasm at 24 and 72 h (Fig. 3B and C). Using water-medium-generated complexes, less than 20% of cells demonstrate fluorescent particles within the cytoplasm with numerous fluorescent spherical clusters observed in the extracellular spaces (Fig. 3D). When the RMG cultures were incubated with naked fluorescent ODN, 18% of the cells showed nuclear fluorescence after 6 h (Fig. 3E). After 24 h of incubation, however, this nuclear fluorescence is not detectable and has faded away (Fig. 3F).

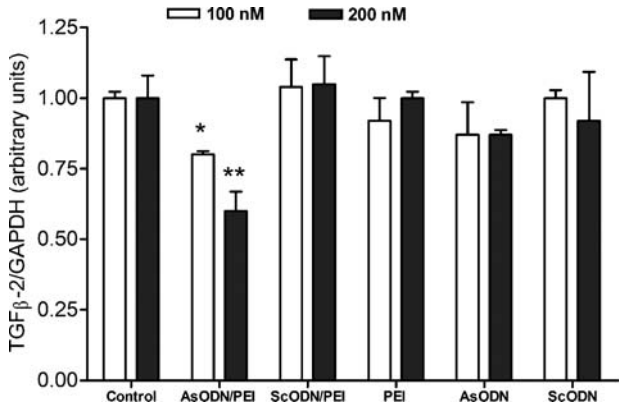

Fig. 5. TGFβ-2 mRNA cell levels were reduced after transfection with complexed antisense TGFβ-2 ODN. RT-PCR assay was performed 72 hours after transfection with complexed (ODN/PEI), naked antisense TGFβ-2 oligonucleotide (ODN) or PEI. Scrambled control sequence was also used in both forms: complexed and naked ODN. ODN concentrations were 100 nM (gray bars) and 200 nM (black bars). PEI concentrations were 9.5 μM (blanc bars) and 19 μM (black bars). Data are the mean ± SD out of three samples. Statistically significant difference *versus* control is shown (*P = 0.030; **P = 0.007).

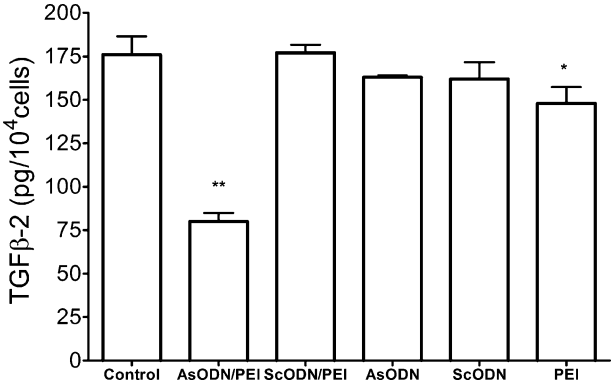

Fig. 6. The production of TGFβ-2 protein cell level was reduced after transfection with antisense TGFβ-2 oligonucleotide complexes. ELISA assay was performed 72 hours after incubation with complexed (ODN/PEI), naked antisenseTGFβ-2 oligonucleotides (ODN) or PEI. Scrambled control sequence was also used in both forms: complexed and naked ODN. ODN concentration was 200 nM; PEI concentration was 19 μM. Results are expressed as percentages of control (untreated cells). Data are the mean ± SD out of three samples. *Statistically significant difference *versus* control (*P = 0.0001; **P = 0.024).

Effect on Cell Viability and Proliferation

As shown in Fig. 4, after 6 h of incubation, naked ODN does not influence cell viability even at the highest concentration (Fig. 4A). Complexes also did not significantly influence cell viability at 100 nM (97 ± 8%, $p = 0.7$) and only slightly decreased the number of living cells at 200 nM (86 ± 5, $p = 0.21$). However, at high complex concentrations (400 nM, corresponding to 38 μM PEI) a significant reduction in the number of living cells was observed (51 ± 4, $p = 0.01$), correlating well to the amount of PEI (Fig. 4B). For all further experiments, 100 nM and 200 nM complexes concentrations were therefore used.

At 72 h, and after 6 h of incubation with complexes prepared with ASODN the number of living cells tended to decrease at 100 nM and was significantly reduced at 200 nM ($p = 0.004$). However, no difference in the number of living cells was observed with complexes prepared with the scrambled ODN, even at the highest concentration (200 nM) (Fig. 4C).

EFFECT ON TGFβ-2 EXPRESSION AND TRANSLATION

As shown in Fig. 5, after transfection, the levels of mRNA TGFβ-2 are lower in RMG cells incubated for 72 h with TGFβ-2 antisense ODN complexes than in similar control cultured cells (Fig. 5). This effect is dose dependent with 20% reduction ($p = 0.03$) and 40% reduction ($p = 0.007$) observed when the cultures are incubated with 100 nM or 200 nM of As-ODN/PEI complexes respectively. RMG cultured cells incubated with scrambled complexes, naked ODN or PEI alone demonstrated TGFβ-2 mRNA expression levels similar to those observed in the control (PBS added) cultures (Fig. 5).

The level of TGFβ-2 protein in RMG culture supernatants are reduced by 47% ($p = 0.0001$) in cultures incubated with 200 nM of complexed As-ODN when

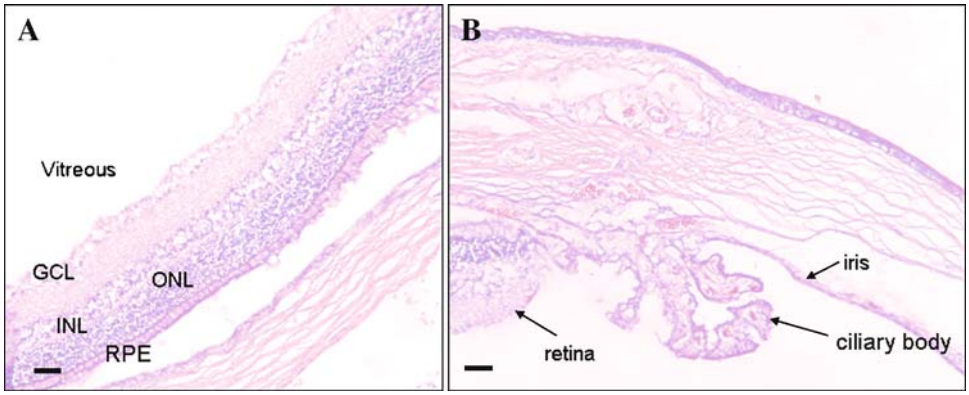

Fig. 7. Histology of retina (A) and ciliary body (B) stained with hematoxylin-eosin at 24 h after injection of complexes. Note that the structure of the retina is normal and that no infiltrating cells are detected in the posterior and anterior segment of the rat eye. Bar = 100 μm.

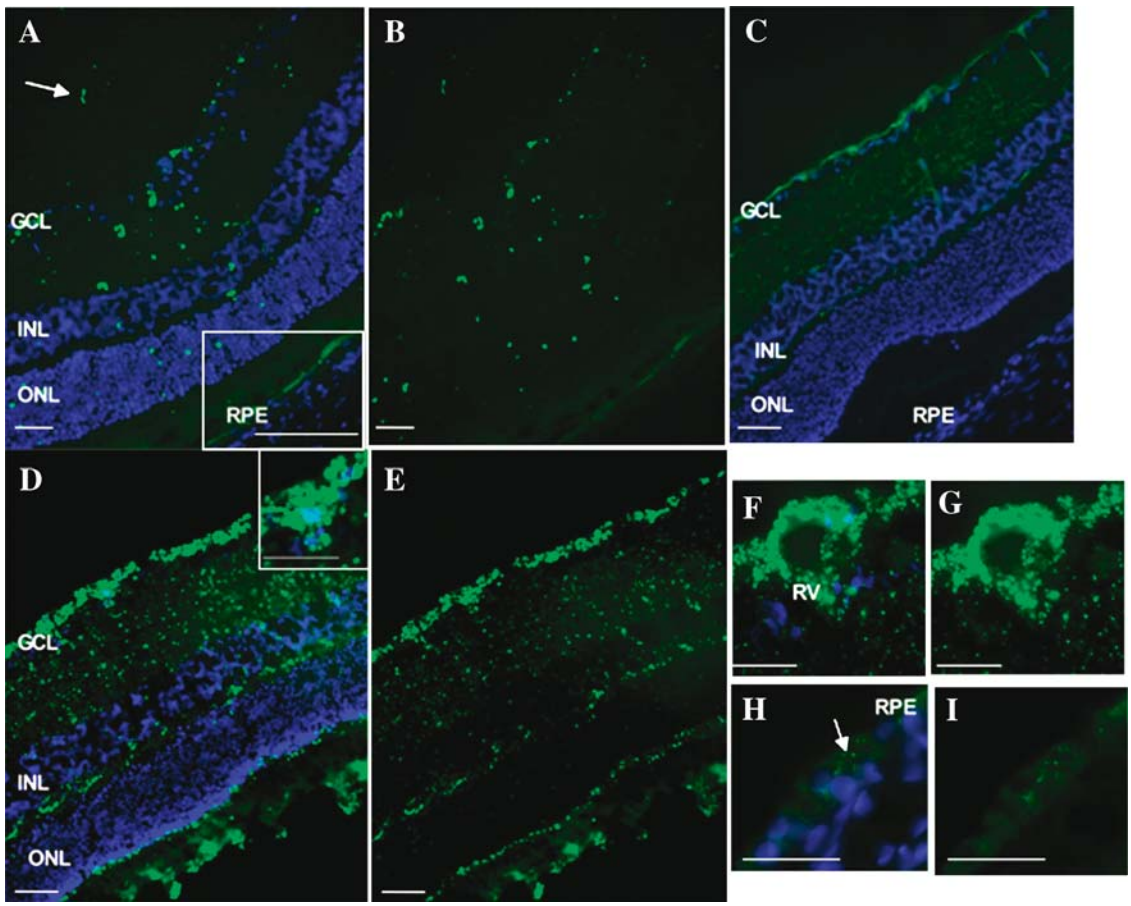

Fig. 8. Fluorescence micrographs of retinal sections 1 and 24 hours after intravitreal injections of complexes and naked ODN. (A–B) 1 hour after intravitreal injections of complexes, green fluorescence (corresponding to FITC ODN) is observed in the vitreous cavity, at the inner limiting, membrane level and the inner nuclear layers (INL). (C) 1 hour after intravitreal injections of fluorescent naked ODN, mostly located at the inner part of the retina. (D–I) 24 hours after intravitreal injections of complexes, fluorescence distribution is homogenously observed all in retinal layers up to the external limiting membrane. High magnifications from (D): a large amount of particles are localized in astrocytes at the retinal inner surface and around retinal vessels (F–G). High magnifications from (A): complexes are also localized in retinal epithelium pigment (RPE) cells at this time point (H–I). Scale bars: (A–E) 10 μm; Scale bars: (F–G) 20 μm; Scale bars: (H–I) 40 μm. Blue fluorescence (DAPI) corresponds to nuclei.

compared to untreated cells (Fig. 6). Incubation of cultures with naked ODN does not affect the levels of TGFβ-2 protein. However, a 15% reduction of TGFβ-2 levels (p = 0.024) is observed when the RMG cell cultures are incubated with PEI alone.

IN VIVO STUDIES

Fate of ODN/PEI Complexes *in Vivo*

ODN/PEI complexes generated in HBS do not induce any clinical or histology signs of ocular inflammation 1 and 24 h after their injection in the vitreous. As shown on sections stained with hematoxylin–eosin, the structure of the retina is strictly normal in eyes injected with complexes and no infiltrating cells can be detected in the retina or in the ciliary body (Fig. 7).

Histology of the eyes 1 h after injections of the ODN/PEI complexes demonstrates the presence of fluorescent nanoparticles in the vitreous cavity, on the inner limiting membrane, and in the retinal inner nuclear layers (Fig. 8A and B). At 24 h, the particles have homogeneously migrated to all retinal layers (Fig. 8D and E). Large numbers of particles are localized in astrocytes at the retinal inner surface and around retinal vessels (Fig. 8F and G). At this time point, fluorescent ODN/PEI complexes are also observed within the RPE cells (Fig. 8H and I). When naked fluorescent ODN was used, a diffuse fluorescence of the inner retina is observed 1 h after the intravitreous injection (Fig. 8C). This fluorescence fades away very rapidly and is not observed when the eyes are examined 24 h after the injection of naked fluorescent ODN (not shown). At 3 days after injection, fluorescent ODN/PEI complexes remained detectable in the retina, particularly in cells located at the inner limiting membrane levels (most probably astrocytes) and in some cell prolongations (Fig. 9A, B, and D), whereas fluorescent nuclei are also observed at the same level (gray arrows). Fluorescent ODNs are also located in nuclei at the inner nuclear layer level (Fig. 9A, C, and B, arrows), most suggestive of free ODNs that have accumulated in retinal Müller cells. Free ODN are injected in the vitreous, at 3 days after injection, no fluorescence can be detected in the retina (Fig. 9C).

Immunohistochemistry

GFAP positive cells were detected at the inner limiting membrane level (Fig. 9E and G), corresponding to astrocytes

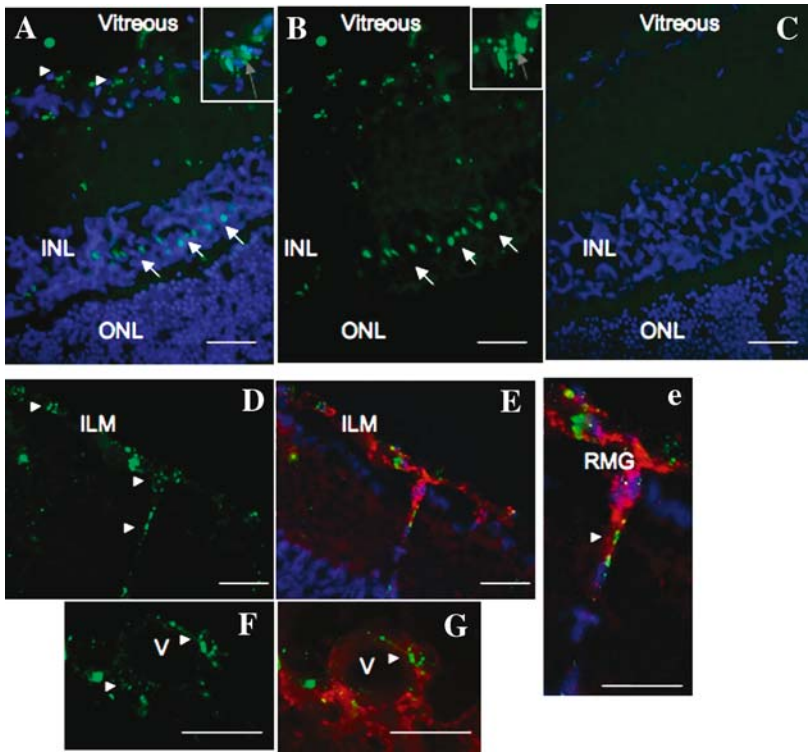

Fig. 9. Fluorescence micrographs and GFAP immunohistochemistry of retinal sections 72 hours after intravitreal injections of complexes and naked ODN. (A, B) After intravitreal injections of complexes, green fluorescence (corresponding to FITC ODN) is observed in the vitreous cavity, at the inner limiting (ILM), membrane level and in the inner nuclear layers (INL). (B) At this time point, fluorescence is located in some nuclei (arrows) in the INL (most suggestive of Retinal Muller Glial cells (RMG) nuclei). (C) Naked ODN, (D, E, e) RMG end feet at the ILM showing complexes formed with FITC ODN (green), GFAP staining specific for glial cells (red) and nuclei (blue). (F, G) Astrocytes around a vessel (V) at the ILM level showing complexes formed with FITC ODN (green) and GFAP staining (red). Scale bars: 20 μm.

and/or to RMG end feet, where complexes could also be detected (Fig. 9D and F) at 3 days after injection. RMG prolongations were occasionally stained with GFAP at 24 h, demonstrating that RMG cells were weakly activated by the injection of complexes. However, in this case, we could localize fluorescent ODN/PEI within RMG prolongations, demonstrating that complexes are efficient to target RMG cells (Fig. 9E, e). Complexes were also observed in astrocytes around large vessels at the optic nerve head (Fig. 9F and G).

DISCUSSION

The goal of this work was to characterize oligonucleotide/polyethylenimine complexes and to evaluate their potential for ocular antisense approach. We have investigated different factors that could influence size and morphology/structure of ODN complexed with PEI.

Our study of ODN/PEI complex characterization has revealed a marked influence of the preparation medium on size distribution. In HBS, we observe a dramatic reduction in both particle size and polydispersity even at high ODN concentrations: 220 nm at N/P 10, 1 mg/mL ODN. These findings reinforce previous results showing formation of small particles (205 nm) using branched PEI with DNA prepared in 50 mM NaCl (25).

In contrast, in water, complexes exhibit a broad polydispersity, suggesting an aggregation phenomenon despite highly positive zeta potential values. Usually, the classical treatment of colloid behavior which assumes the tendency of a particulate system to aggregate is largely determined by electrostatic interactions: Positively or negatively charged particles possessing an electrostatic potential greater than the potential energy of their Van der Waals interaction are thought to be stable against aggregation (26). In line with the positive charge found in our work, early evidence showed that some complexes with highly positive zeta potential can actually form clusters in aqueous media (26,27). The aggregates seem to be formed by small spherical particles (20–50 nm) corresponding to complexes confined within a large polymeric network and conferring the positive charge. The ability to form clusters has also been observed by Tang and Szoka (26) for DNA, and this phenomenon was mainly influenced by the type of cationic polymer used.

Using different imaging techniques (TEM, SEM, and FFEM), we have demonstrated that the preparation medium not only influences the particle size and polydispersity but also determines its structure. An anisotropic shell should be birefringent enough to generate the observed Malta crosses, and is consequently in agreement with a core–shell structure for complexes prepared in HBS. The different structures observed in pure water or in HBS could be derived from the conformation of PEI in these media. Indeed, in water, PEI is fully spread and forms a network on which ODN can be complexed into small particles that are visible on Fig. 2C. On the contrary, in PBS due to the electrostatic screening, PEI may be organized into more compact coils, and probably ODN may be complexed with PEI at the interface of the coil. The charge ratio is in favor of cationic charges; therefore, it is not surprising to obtain positively charged particles with zeta potential measurements (28).

In the literature, the general principles governing nucleic acid morphology complexation remain essentially vague (29). First, the precipitation phenomenon differs from DNA condensation, defined as the collapse of DNA to aggregates/precipitates of defined size and orderly morphology (30). Second, DNA condensation is mainly found with duplex DNA (size larger than 400 bp), whereas precipitation is observed even with very short single-strand DNA (21 bp) (31). Third, condensation to toroids, rods, or spheroids that are between 50 and 300 nm in diameter can be achieved for DNA in the presence of multivalent cations, including polymers such as PEI, but well-defined structures in presence of ODN have been less studied (29). In this respect, we described the ODN/PEI complex structure as a spheroid nanoparticle.

The size and morphology of the complexes also influence the transfection potential of the complexes, with a higher transfection rate observed for complexes prepared in HBS. The large aggregates observed with complexes prepared in water may explain their low cellular internalization potential.

A critical step in the delivery of ODN complexes is their ability to dissociate, releasing the transported ODN within the target cell. If the affinity between the ODN and the cationic carriers is too low, the complex will dissociate prematurely. On the other hand, a strong affinity might prevent the release of the ODN once the complex is already in the cytoplasm. Thus, an optimal balance between the formed particle size and the affinity of the trapped ODN within the formed particle has to be the aim.

From RMG cell viability assay, we determined that the maximal tolerated (nontoxic) PEI concentration is around 19 μM and that up to 200 nM ODN/PEI complexes can be safely be used. We therefore have evaluated the down-regulation of TGFβ-2 and potential effect on cell proliferation using 200 and 100 nM concentrations. In RMG cells *in vitro*, the ODN created in HBS induced a dose-dependent effect with around 40% down-regulation of TGFβ-2 mRNA and a 47% inhibition of TGFβ-2 protein expression after an incubation period of 72 h. Correlating well with these results, inhibition of cell growth is observed at 72 h using 200 nM concentration. Interestingly, no inhibition of cell growth can be detected at 72 h when the scrambled ODN is used, demonstrating that the complexes do not induce a nonspecific inhibition of cell growth that could be related to a toxic effect. These findings demonstrate that the complexes internalized within the cells are stable and able to release functional ODNs. In contrast, the naked ODN had no effect on TGFβ-2 expression, demonstrating that the formation of complexes is the critical point to induce the antisense effect. The decrease of TGFβ-2 expression and translation levels using As-ODN nanoparticles was specific because nanoparticles formed with scrambled ODN sequences did not influence TGFβ-2 expression or production. Jääskeläinen *et al.* did not observe any down-regulation of gene expression 24 h after transfection with ODN complexed with branched PEI (32), which is in line with our observations. Our present study indeed confirms that down-regulation does not occur early after transfection but is observed only after 72 h. This delayed ODN activity is probably associated with the relative strong affinity between the ODN and the PEI within the complex and the resulting slow release of the "trapped" ODN.

The exact role of TGFβ-2 on RMG cell proliferation and transdifferentiation remains incompletely elucidated and controversial. In human RMG cell cultures, the addition of exogenous TGFβ-2 did not affect the basal RMG cell proliferation but inhibited the basic fibroblast growth factor (bFGF)-, platelet-derived growth factor (PDGF)-, or epidermal growth factor (EGF)-induced RMG proliferation (33). In experimental PVR, experimentally detached retina and during the formation of retinal membranes, high levels of TGFβ are found in the vitreous (34). Moreover, in a rabbit model of PVR, blocking the generation of TGFβ-2 using specific soluble receptors prevented the development of fibrovascular membranes demonstrating that anti-TGFβ strategies have potential interests in the treatment of proliferative retinal diseases (19). Therefore, we have evaluated the fate and tolerance of ODN/PEI complexes after intravitreous injection in the normal rat.

Twenty-four hours after their injection, the complexes migrate in glial cells at the surface of the retina and distribute homogeneously in all retinal layers. In this regard, ODN/PEI nanoparticle complexes behave like other peptidic nanoparticles (35), probably due to their shape and size. Costaining with GFAP confirmed that astrocytes and RMG cells are able to internalize ODN/PEI complexes. Interestingly, 72 h after intravitreous injection, whereas complexes can still be observed in the retina and in glial cells, fluorescence concentrated in nuclei of the superficial retinal layer and in the inner nuclear layer, which is in favor of the release of free ODN in the targeted cells.

In summary, we have found that the use of HBS and appropriate ODN/PEI ratio are optimal conditions for the formation of well-defined, stable, and low-toxic ODN/PEI nanoparticle complexes. These complexes have been used to deliver specific As-ODN directed at TGFβ-2 to cultured RMG cells, inducing specific down-regulation of the expression and production of TGFβ-2. Our preliminary *in vivo* experiments show that ODN/PEI nanoparticle complexes may be used to efficiently transfect retinal glial cells. These findings and their potential therapeutic aspects are currently under investigation in our laboratory.

ACKNOWLEDGMENTS

We gratefully acknowledge Dr. C. Deloménie from Plate-forme Transcriptome (INSERM IFR-75 ISIT), Dr. D. Jaillard (UMR CNRS 8080, CCME, Université Paris-Sud), Dr. H. Alphandary (UMR CNRS 8612), Dr. F. Garnier (Ecole Centrale Paris), G. Frebourg. and Dr. J.-P. Lechaire (UMR CNRS 7622, Université Pierre et Marie Curie) for their technical assistance. Ana L. G. Santos was supported by a fellowship from Fundação Coordenação de Aperfeiçoamento de Pessoal de Nível Superior-CAPES (Brazil). We also acknowledge the "Fondation pour l'Avenir" and EviGenoRet LSHG-CT-2005-512036 for funding of this work.

REFERENCES

1. C. F. Bennett. Antisense oligonucleotide therapeutics. *Expert Opin. Investig. Drugs* **8**:237–253 (1999).
2. S. Akhtar and R. L. Juliano. Cellular uptake and intracellular fate of antisense oligonucleotides. *Trends Cell. Biol.* **2**:139–144 (1992).
3. S. Capaccioli, G. Di Pasquale, E. Mini, T. Mazzei, and A. Quattrone. Cationic lipids improve antisense oligonucleotide uptake and prevent degradation in cultured cells and in human serum. *Biochem. Biophys. Res. Commun.* **197**:818–825 (1993).
4. J. G. Lewis, K. Y. Lin, A. Kothavale, W. M. Flanagan, M. D. Matteucci, R. B. DePrince, R. A. Mook Jr., R. W. Hendren, and R. W. Wagner. A serum-resistant cytofectin for cellular delivery of antisense oligodeoxynucleotides and plasmid DNA. *Proc. Natl. Acad. Sci. USA* **93**:3176–3181 (1996).
5. H. Yoo and R. L. Juliano. Enhanced delivery of antisense oligonucleotides with fluorophore-conjugated PAMAM dendrimers. *Nucleic Acids Res.* **28**:4225–4231 (2000).
6. D. Lochmann, E. Jauk, and A. Zimmer. Drug delivery of oligonucleotides by peptides. *Eur. J. Pharm. Biopharm.* **58**:237–251 (2004).
7. R. M. Orr. Technology evaluation: fomivirsen, Isis Pharmaceuticals Inc/CIBA vision. *Curr. Opin. Mol. Ther.* **3**:288–294 (2001).
8. A. Bochot, E. Fattal, A. Gulik, G. Couarraze, and P. Couvreur. Liposomes dispersed within a thermosensitive gel: a new dosage form for ocular delivery of oligonucleotides. *Pharm. Res.* **15**:1364–1369 (1998).
9. A. Bochot, E. Fattal, V. Boutet, J. R. Deverre, J. C. Jeanny, H. Chacun, and P. Couvreur. Intravitreal delivery of oligonucleotides by sterically stabilized liposomes. *Invest. Ophthalmol. Vis. Sci.* **43**:253–259 (2002).
10. R. A. Bejjani, D. BenEzra, H. Cohen, J. Rieger, C. Andrieu, J. C. Jeanny, G. Gollomb, and F. F. Behar-Cohen. Nanoparticles for gene delivery to retinal pigment epithelial cells. *Mol. Vis.* **11**:124–132 (2005).
11. J. Scherer and J. Schnitzer. Growth factor effects on the proliferation of different retinal glial cells *in vitro*. *Brain Res. Dev. Brain Res.* **80**:209–221 (1994).
12. C. H. Kon, N. L. Occleston, G. W. Aylward, and P. T. Khaw. Expression of vitreous cytokines in proliferative vitreoretinopathy: a prospective study. *Invest. Ophthalmol. Vis. Sci.* **40**:705–712 (1999).
13. E. H. Lee, Y. Seomun, K. H. Hwang, J. E. Kim, I. S. Kim, J. H. Kim, and C. K. Joo. Overexpression of the transforming growth factor-beta-inducible gene betaig-h3 in anterior polar cataracts. *Invest. Ophthalmol. Vis. Sci.* **41**:1840–1845 (2000).
14. O. Nishi, K. Nishi, K. Wada, and Y. Ohmoto. Expression of transforming growth factor (TGF)-alpha, TGF-beta(2) and interleukin 8 messenger RNA in postsurgical and cultured lens epithelial cells obtained from patients with senile cataracts. *Graefes Arch. Clin. Exp. Ophthalmol.* **237**:806–811 (1999).
15. F. F. Behar-Cohen, B. Thillaye-Goldenberg, T. de Bizemont, M. Savoldelli, D. Chauvaud, and Y. Kozakde. EIU in the rat promotes the potential of syngeneic retinal cells injected into the vitreous cavity to induce PVR. *Invest. Ophthalmol. Vis. Sci.* **41**:3915–3924 (2000).
16. T. B. Connor Jr., A. B. Roberts, M. B. Sporn, D. Danielpour, L. L. Dart, R. G. Michels, S. Bustrosde, C. Enger, H. Kato, and M. Lansing. Correlation of fibrosis and transforming growth factor-beta type 2 levels in the eye. *J. Clin. Invest.* **83**:1661–1666 (1989).
17. G. A. Lutty, C. Merges, A. B. Threlkeld, S. Crone, and D. S. McLeod. Heterogeneity in localization of isoforms of TGF-beta in human retina, vitreous, and choroid. *Invest. Ophthalmol. Vis. Sci.* **34**:477–487 (1993).
18. L. R. Pasquale, M. E. Dorman-Pease, G. A. Lutty, H. A. Quigley, and H. D. Jampel. Immunolocalization of TGF-beta 1, TGF-beta 2, and TGF-beta 3 in the anterior segment of the human eye. *Invest. Ophthalmol. Vis. Sci.* **34**:23–30 (1993).
19. Y. Oshima, T. Sakamoto, T. Hisatomi, C. Tsutsumi, H. Ueno, and T. Ishibashi. Gene transfer of soluble TGF-beta type II receptor inhibits experimental proliferative vitreoretinopathy. *Gene Ther.* **9**:1214–1220 (2002).
20. M. F. Cordeiro, A. Mead, R. R. Ali, R. A. Alexander, S. Murray, C. Chen, C. York-Defalco, N. M. Dean, G. S. Schultz, and P. T. Khaw. Novel antisense oligonucleotides targeting TGF-beta

inhibit *in vivo* scarring and improve surgical outcome. *Gene Ther.* **10**:59–71 (2003).
21. F. Ungaro, G. De Rosa, A. Miro, and F. Quaglia. Spectrophotometric determination of polyethylenimine in the presence of an oligonucleotide for the characterization of controlled release formulations. *J. Pharm. Biomed. Anal.* **31**:143–149 (2003).
22. A. Richard, V. Marchi-Artzner, M. N. Lalloz, M. J. Brienne, F. Artzner, T. Gulik-Krzywicki, M. A. Guedeau-Boudeville, and J. M. Lehn. Fusogenic supramolecular vesicle systems induced by metal ion binding to amphiphilic ligands. *Proc. Natl. Acad. Sci. USA* **101**:15279–15284 (2004).
23. Y. de Kozak, M. C. Naud, J. Bellot, J. P. Faure, and D. Hicks. Differential tumor necrosis factor expression by resident retinal cells from experimental uveitis-susceptible and -resistant rat strains. *J. Neuroimmunol.* **55**:1–9 (1994).
24. J. L. Bourges, S. E. Gautier, F. Delie, R. A. Bejjani, J. C. Jeanny, R. Gurny, D. BenEzra, and F. F. Behar-Cohen. Ocular drug delivery targeting the retina and retinal pigment epithelium using polylactide nanoparticles. *Invest. Ophthalmol. Vis. Sci.* **44**:3562–3569 (2003).
25. L. Wightman, R. Kircheis, V. Rossler, S. Carotta, R. Ruzicka, M. Kursa, and E. Wagner. Different behavior of branched and linear polyethylenimine for gene delivery *in vitro* and *in vivo*. *J. Gene Med.* **3**:362–372 (2001).
26. M. X. Tang and F. C. Szoka. The influence of polymer structure on the interactions of cationic polymers with DNA and morphology of the resulting complexes. *Gene Ther.* **4**:823–832 (1997).
27. S. C. De Smedt, J. Demeester, and W. E. Hennink. Cationic polymer based gene delivery systems. *Pharm. Res.* **17**:113–126 (2000).
28. G. B. Kramer, H. M. Buchhamer and K. Lunkwitz. Surface modification by polyelectrolyte complexes: influence of different polyelectrolyte components and substrates. *Coll. Surf.* **A122**: 1–12 (1997).
29. V. Vijayanathan, T. Thomas, and T. J. Thomas. DNA nanoparticles and development of DNA delivery vehicles for gene therapy. *Biochemistry* **41**:14085–14094 (2002).
30. V. A. Bloomfield. DNA condensation by multivalent cations. *Biopolymers* **44**:269–282 (1997).
31. M. Saminathan, T. Antony, A. Shirahata, L. H. Sigal, T. Thomas, and T. J. Thomas. Ionic and structural specificity effects of natural and synthetic polyamines on the aggregation and resolubilization of single-, double-, and triple-stranded DNA. *Biochemistry* **38**:3821–3830 (1999).
32. I. Jääskeläinen, S. Peltola, P. Honkakoski, J. Monkkonen, and A. Urtti. A lipid carrier with a membrane active component and a small complex size are required for efficient cellular delivery of anti-sense phosphorothioate oligonucleotides. *Eur. J. Pharm. Sci.* **10**:187–193 (2000).
33. T. Ikeda and D. G. Puro. Regulation of retinal glial cell proliferation by antiproliferative molecules. *Exp. Eye Res.* **60**:435–443 (1995).
34. C. J. Guerin, L. Hu, G. Scicli, and A. G. Scicli. Transforming growth factor beta in experimentally detached retina and periretinal membranes. *Exp. Eye Res.* **73**:753–764 (2001).
35. N. Normand, F. Valamanesh, M. Savoldelli, F. Mascarelli, D. BenEzra, Y. Courtois, and F. Behar-Cohen. VP22 light controlled delivery of oligonucleotides to ocular cells *in vitro* and *in vivo*. *Mol. Vis.* **11**:184–191 (2005).